Hindawi Publishing Corporation
International Journal of Photoenergy
Volume 2015, Article ID 320625, 6 pages
http://dx.doi.org/10.1155/2015/320625

Research Article

Wetting and Photocatalytic Properties of TiO_2 Nanotube Arrays Prepared via Anodic Oxidation of E-Beam Evaporated Ti Thin Films

Soon Wook Kim,[1] Hong Ki Kim,[1] Jong Won Yun,[1] Eui Jung Kim,[2] and Sung Hong Hahn[1]

[1]*Department of Physics, University of Ulsan, Ulsan 680-749, Republic of Korea*
[2]*Department of Chemical Engineering, University of Ulsan, Ulsan 680-749, Republic of Korea*

Correspondence should be addressed to Eui Jung Kim; ejkim@ulsan.ac.kr and Sung Hong Hahn; shhahn@ulsan.ac.kr

Received 28 July 2015; Accepted 30 September 2015

Academic Editor: Xuxu Wang

TiO_2 nanotube arrays (TNAs) are fabricated on quartz substrate by anodizing E-beam evaporated Ti films. E-beam evaporated Ti films are directly anodized at various anodizing voltages ranging from 20 to 45 V and their morphological, wetting, and photocatalytic properties are examined. The photocatalytic activity of the prepared TNAs is evaluated by the photodecomposition of methylene blue under UV illumination. The TNAs prepared at an anodizing voltage of 30 V have a high roughness of 30.1 nm and a low water contact angle of 7.5°, resulting in a high photocatalytic performance. The surface roughness of the TNAs is found to correlate inversely with the water contact angle. High roughness (i.e., high surface area), which leads to high hydrophilicity, is desirable for effective photocatalytic activity.

1. Introduction

TiO_2 has been actively studied as photocatalytic material due to its large band-gap (anatase: 3.2 eV), stable, and nontoxic nature [1–4]. To improve the photocatalytic property of TiO_2, several methods have been considered such as controlling band-gap energy through doping nonmetal materials [5–8] and enlarging the surface area by producing TiO_2 in the form of wire, rod, and particle [9, 10]. TiO_2 nanotube (TNA) is known to have a high photo collection efficiency and large surface area/volume ratio, and it can be easily filled with liquid thus enabling intimate contact with dye and electrolyte [11–14].

Commonly, TNAs can be formed via anodic oxidation of Ti foil by applying a potential to the anode connected to the Ti foil in the electrolyte. The diameter of the TNAs can be controlled by changing the anodizing voltage [15]. This method of using the Ti foil requires a subsequent process like peeling off the TNAs from the Ti foil. However, it is difficult to separate large-area TNAs without cracking. Furthermore, this method requires an additional process to attach the separated TNAs to substrate in order to fabricate the device.

In this work, we prepared Ti films using an E-beam evaporation method and investigated relationship between roughness, hydrophilicity, and photocatalytic performance. E-beam evaporated Ti thin films were anodized at various applied voltages and annealed at different temperatures. The prepared TNAs were characterized using various techniques such as field emission scanning electron microscopy (FE-SEM), water contact angle goniometry, X-ray diffraction (XRD) spectroscopy, and photocatalysis. The TNAs prepared at an applied voltage of 30 V showed the best photocatalytic properties for the photodegradation of methylene blue under black-light irradiation.

2. Material and Methods

The TNAs were prepared by anodizing Ti thin films on the quartz glass substrate using an E-beam evaporator (Temescal FC-2000, USA) with a Ti tablet (99.99% pure). Prior to deposition, the E-beam evaporator was evacuated to a base pressure of 4×10^{-7} Torr. The electron gun voltage and the current were 9.96 kV and 115 mA, respectively. The deposition

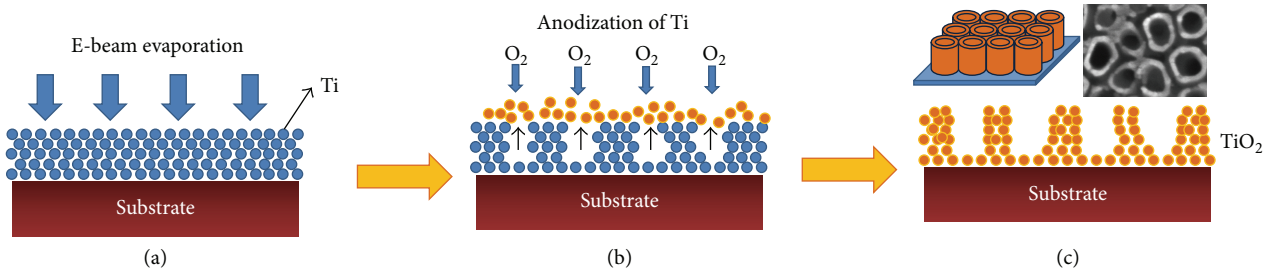

FIGURE 1: A schematic diagram for the preparation of TNAs: (a) deposition of Ti thin film on quartz substrate using E-beam evaporation method, (b) anodic oxidation of Ti thin film, and (c) formation of TNAs.

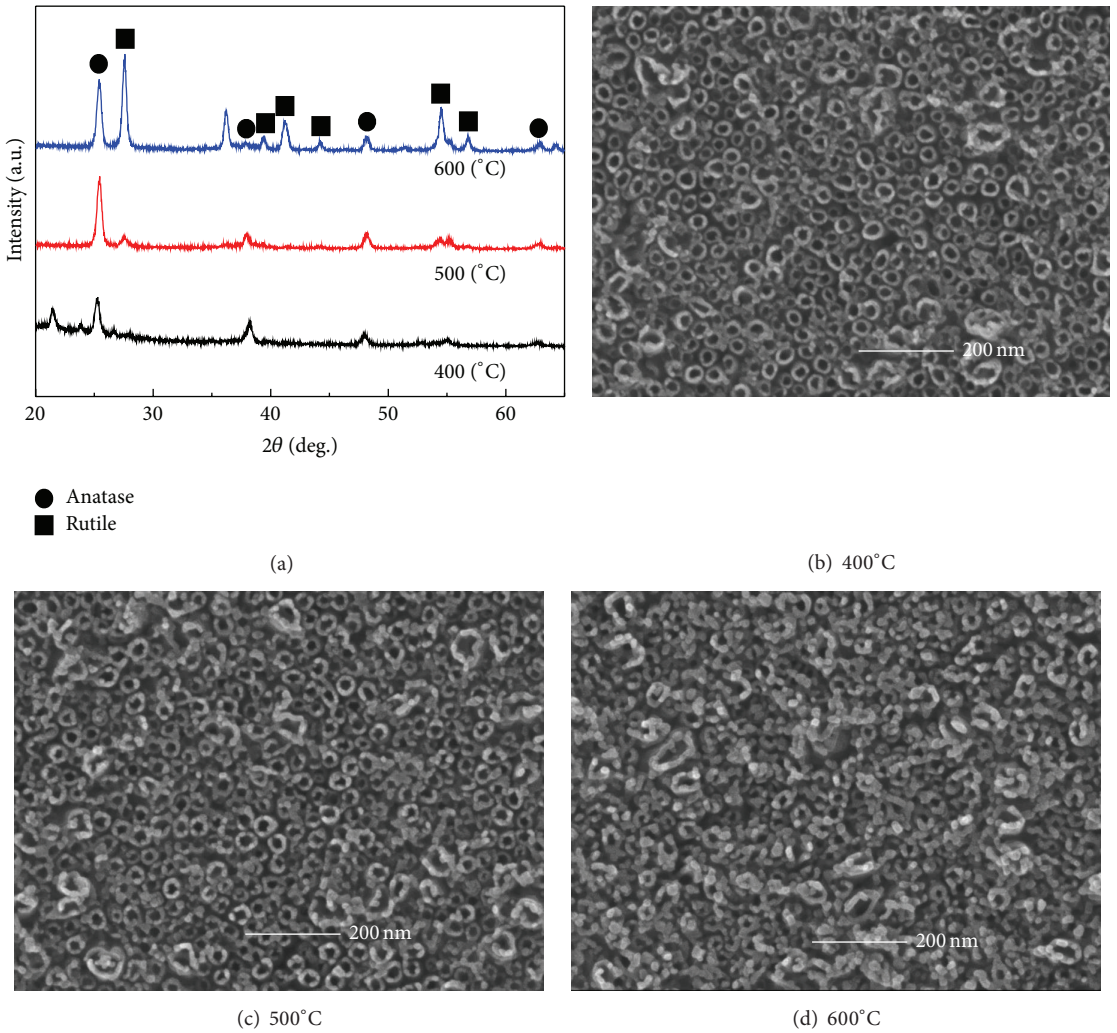

FIGURE 2: XRD patterns and surface SEM images of TNAs annealed at 400°C, 500°C, and 600°C.

rate was 0.5 nm/s and the substrate was rotated at 20 rpm to obtain uniform Ti films. The Ti thin films were anodized in a mixture of glycerol, NH_4F (0.2 wt%), and H_2O (2.5 vol%) as an electrolyte using a carbon counter electrode for 2 h to form the TNAs and then cooled from room temperature to 10°C using a WiseCircu fuzzy control system to enhance the binding force of the TNAs. The samples prepared at an applied anodizing voltage of 20 V, 25 V, 30 V, 35 V, 40 V, and 45 V are referred to as T20, T25, T30, T35, T40, and T45, respectively. To compare with the TNAs, TiO_2 thin film was prepared by using an E-beam evaporation method. After the E-beam evaporator was evacuated to a base pressure of 6×10^{-6} Torr, TiO_2 thin films were deposited at a working oxygen gas pressure of 5×10^{-5} Torr and a temperature of 200°C. The electron gun voltage was 7.0 kV and the current was 200 mA for the TiO_2 film deposition. The substrate was

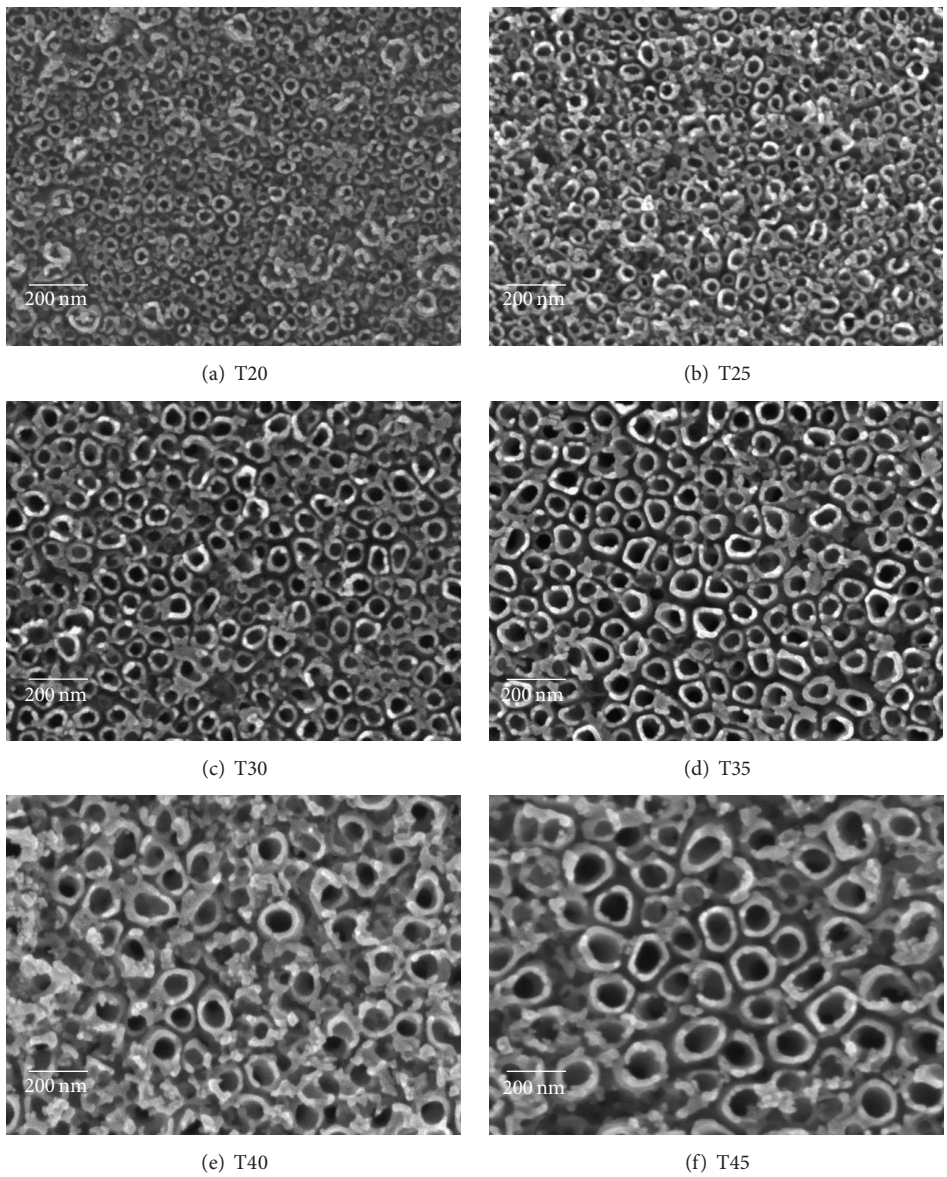

(a) T20 (b) T25

(c) T30 (d) T35

(e) T40 (f) T45

Figure 3: Top-view SEM images of TNAs prepared at different anodizing voltages.

rotated at 15 rpm to obtain uniform TiO_2 films. The samples were annealed at 500°C for 2 h.

The surface morphology of the TNAs was examined using FESEM (JSM-6500F, JEOL). The crystalline structure was determined by XRD spectroscopy (PW3710, Philips) with Kα radiation ($\lambda = 1.5406$ Å). The surface hydrophilicity was evaluated using contact angle goniometry. To test their photocatalytic activities, the TNA thin films (2.0×2.0 cm^2) were immersed in 10 mL of 10^{-5} M methylene blue ($C_{16}H_{18}N_3S$-Cl-$3H_2O$) solution and irradiated with 4 surrounding 20 W black-light (UVA) lamps (wavelength range: 315–400 nm). The photocatalytic performance of the samples was evaluated by measuring the absorbance of the methylene blue solution at 665 nm using a UV-Vis spectrophotometer (HP8453).

3. Results and Discussion

Figure 1 shows the growth mechanism of TNAs prepared by anodic oxidation of E-beam evaporated Ti thin film. Firstly, the Ti thin film was deposited by E-beam evaporation (Figure 1(a)). The titanium was anodized to TiO_2 by reacting with H_2O at the interface. The TiO_2 thin film as a barrier layer is formed on the surface of the Ti film. Then, it was etched by F^- ions developing holes in the TiO_2 film (Figure 1(b)). Chemical reactions involved in the etching of the Ti film are as follows:

$$\begin{aligned} Ti^{4+} + 2H_2O &\longrightarrow TiO_2 + 4H^+ + 4e^- \\ TiO_2 + 6F^- + 4H^+ &\longrightarrow [TiF_6]^{2-} + 2H_2O \end{aligned} \quad (1)$$

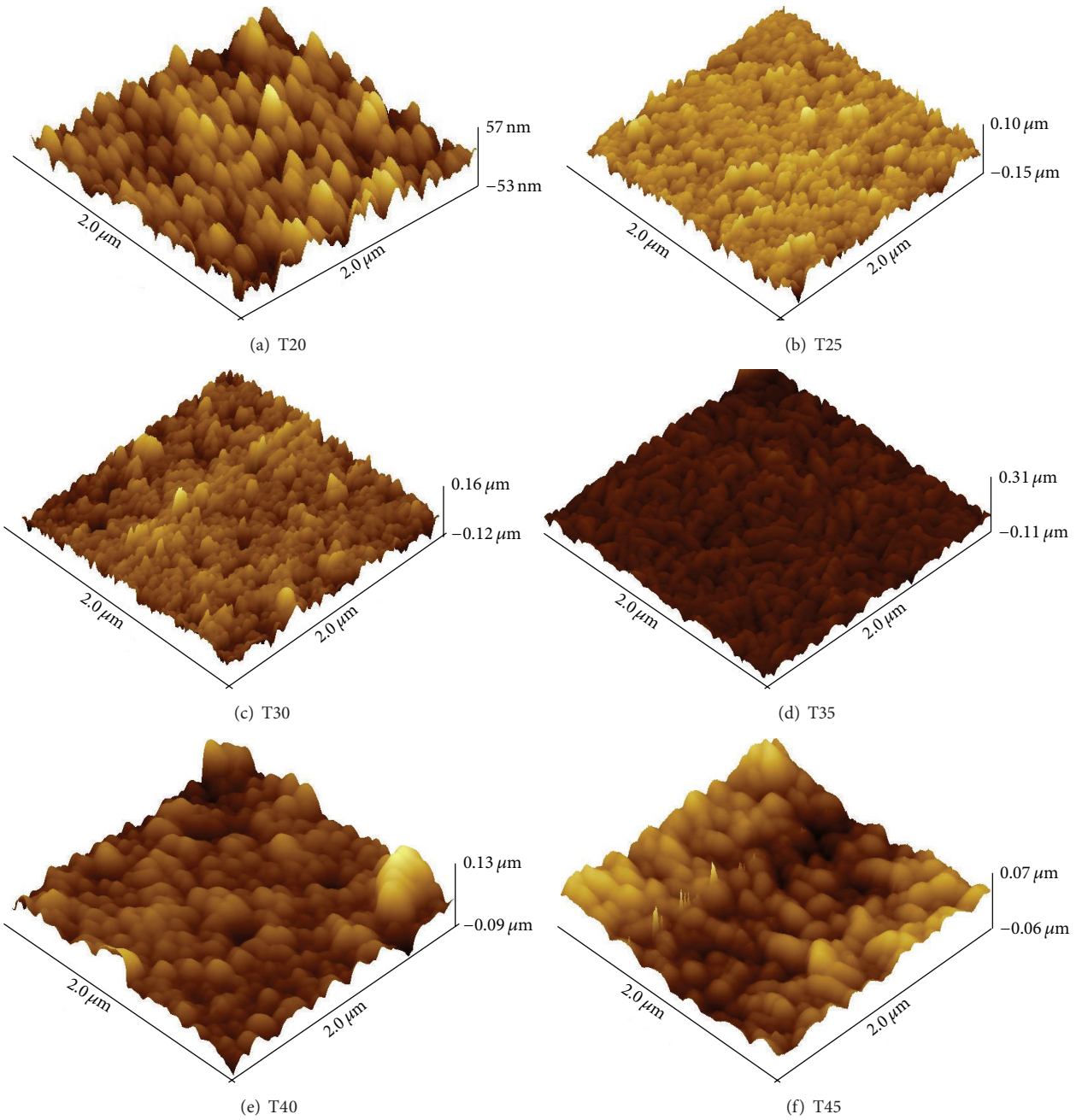

Figure 4: AFM images of TNAs prepared at different anodizing voltages.

As the reaction proceeds, the holes grow deeper into the TiO_2 film and the metallic regions at the pore, leading to the formation of the nanotube structure (Figure 1(c)).

Figure 2 shows the XRD patterns and SEM images of TNAs anodized at 20 V and annealed at 400, 500, and 600°C. The anatase and rutile phases of TiO_2 were identified from XRD patterns in Figure 2(a). After annealing at 400°C, only anatase phase peaks appeared at 25.3°, 38.7°, and 54.1° which correspond to (101), (004), and (105) planes, respectively (JCPDS number 01-089-4921). The intensity of the major anatase peak at 25.3° was increased with increasing annealing temperature from 400°C to 500°C indicating improved crystallinity at 500°C. As the annealing temperature was further increased to 600°C, rutile phase peaks at 27.5° and 36.2° which are consistent with JCPDS number 01-078-2485 appeared in the XRD pattern. The SEM images of the samples in Figures 2(b)–2(d) show the morphological properties of TNAs with different annealing temperatures. In Figures 2(b)-2(c), the TNAs were fairly uniform in shape and size. At 600°C (Figure 2(d)), the TNAs were nonuniform in size and shape (Figures 2(c) and 2(d)). Due to the appearance of rutile phase, the surface coarsening took place and the grain size increased. These results may cause a decreased photocatalytic activity of the sample [16]. In this study,

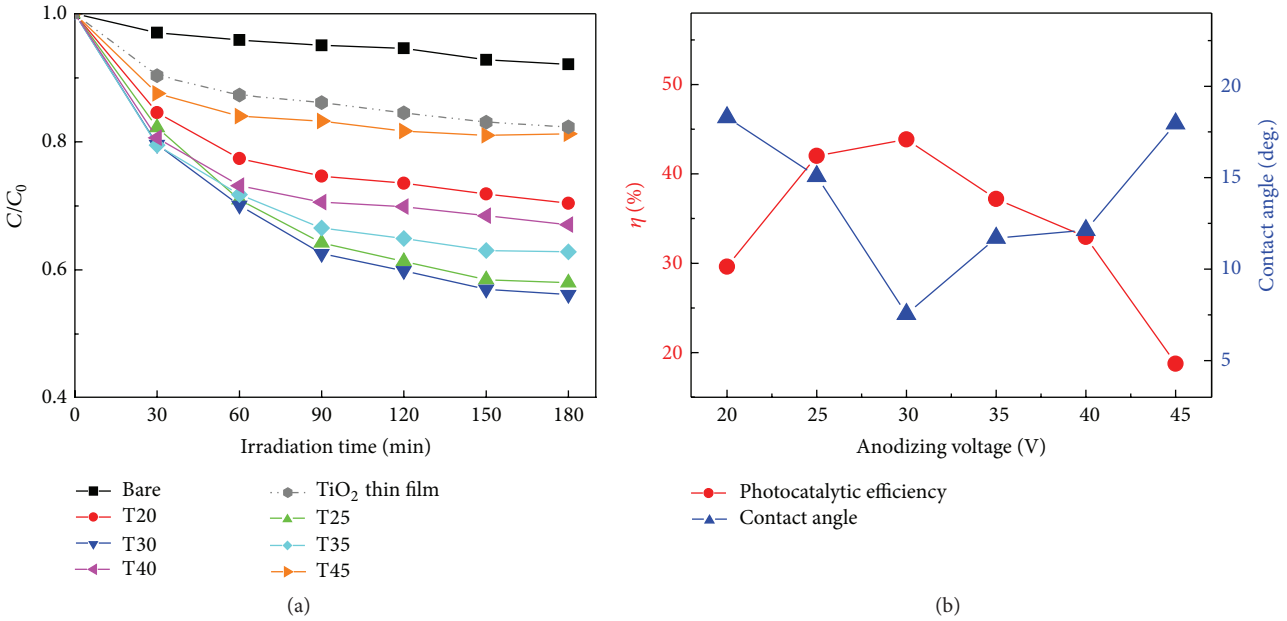

FIGURE 5: (a) Variations of methylene blue concentration with UV irradiation time for the samples. (b) Photocatalytic efficiency and water contact angle of TNA film as a function of anodizing voltage.

we employed the 500°C-annealed TNAs with anatase phase and good crystallinity to investigate their structural, wetting, and photocatalytic properties by changing the anodizing voltage in synthesizing the TNAs.

Figure 3 illustrates the SEM images of TNAs prepared at different anodizing voltages from 20 to 45 V. The TNA samples prepared at an anodizing voltage of 20 V, 25 V, 30 V, 35 V, 40 V, and 45 V are referred to as T20, T25, T30, T35, T40, and T45, respectively. The average inner diameter of the T20, T25, T30, T35, T40, and T45 samples was 23.1 nm, 28.8 nm, 42.4 nm, 57.8 nm, 68.4 nm, and 62.2 nm, respectively. The inner diameter increased with increasing anodizing voltage and the average wall thickness of the tubes also increased from 9.0 to 21.8 nm as the anodizing voltage was increased from 20 V to 45 V. From the AFM images (Figure 4), the roughness of the samples was determined as 15.4 nm, 24.7 nm, 30.1 nm, 20.7 nm, 20.5 nm, and 19.1 nm for the T20, T25, T30, T35, T40, and T45, respectively. As can be seen in Table 1, the 30 V-anodized sample had the lowest contact angle of 7.5° and the 20 V- and 45 V-anodized ones had high values of 18.3° and 18.0°, respectively. The water contact angle was found to correlate inversely with the roughness. According to the Wenzel theory, a lower water contact angle indicates a higher hydrophilicity [17]. This means that a rough surface can be more hydrophilic than a smooth surface.

The photocatalytic performance of the samples was evaluated by the photodecomposition of methylene blue under black-light irradiation. Figure 5(a) shows variations of methylene blue concentration with UV irradiation time for TiO_2 film and TNA films prepared at different anodizing voltages. The concentration of methylene blue was determined from the UV-Vis absorbance at 644 nm. The TNA films displayed better photodecomposition ability than the TiO_2 film. The 30 V-anodized TNAs exhibited the best photocatalytic performance. Figure 5(b) shows the photocatalytic efficiency and water contact angle of TNA film as a function of anodizing voltage. The photocatalytic efficiency, η, is defined as $(C_0 - C)/C_0 \times 100(\%)$, where C_0 is the initial concentration of methylene blue and C is its concentration after 180 min of UV illumination. The 30 V-anodized TNAs had the highest photocatalytic decomposition efficiency of 43.9%, while the 45 V-anodized TNAs had the lowest efficiency of 18.8%. Rough surface (large surface area) and high hydrophilicity make water easily get into the inside of the tube. Accordingly, a high surface area and hydrophilicity would be desirable for achieving an excellent photocatalytic activity toward organic pollutant degradation (Figure 5(b)). The results of Figure 5 demonstrate that a hydrophilic surface is favorable to enhanced photocatalytic performance.

TABLE 1: Roughness, wetting energy, and water contact angle of TNAs prepared at different anodizing voltages.

	20 V	25 V	30 V	35 V	40 V	45 V
Roughness (nm)	15.4	24.7	30.1	20.7	20.5	19.1
Wetting energy (mN/m)	69.1	70.3	72.2	71.3	71.5	69.4
Water contact angle (°)	18.3	15.1	7.5	11.7	12.1	18.0

4. Conclusion

We have developed an effective method for preparing TNAs by anodizing E-beam evaporated Ti thin film and investigated the structural, hydrophilic, and photocatalytic properties of the TNAs prepared at different anodizing voltages ranging

from 20 V to 45 V. The TNAs had anatase phase after annealing at 500°C and rutile phase at 600°C. The inner tube diameter of the TNAs increased from 23.1 nm to 62.2 nm with increasing anodizing voltage from 20 V to 45 V. The 30 V-anodized TNAs had the highest roughness of 30.1 nm and the lowest contact angle of 7.5°, resulting in the highest photocatalytic activity. The TNAs with a rough surface were more hydrophilic than those with a smooth surface, demonstrating that high surface area and hydrophilicity are crucial to photocatalytic activity.

Conflict of Interests

All authors declare that there is no conflict of interests regarding the publication of this paper.

Authors' Contribution

Soon Wook Kim and Hong Ki Kim contributed equally to this work.

Acknowledgments

This research was financially supported by the Ministry of Education (MOE) and National Research Foundation of Korea (NRF) through the Human Resource Training Project for Regional Innovation (2012H1B8A2026179) and the Basic Science Research Program (2012R1A1A4A01015466).

References

[1] X. Pang, W. Chang, C. Chen, H. Ji, W. Ma, and J. Zhao, "Determining the TiO_2-photocatalytic aryl-ring-opening mechanism in aqueous solution using oxygen-18 labeled O_2 and H_2O," *Journal of the American Chemical Society*, vol. 136, no. 24, pp. 8714–8721, 2014.

[2] P. Wang, J. Wang, T. Ming et al., "Dye-sensitization-induced visible-light reduction of graphene oxide for the enhanced TiO_2 photocatalytic performance," *ACS Applied Materials and Interfaces*, vol. 5, no. 8, pp. 2924–2929, 2013.

[3] S. Suzuki, T. Tsuneda, and K. Hirao, "A theoretical investigation on photocatalytic oxidation on the TiO_2 surface," *Journal of Chemical Physics*, vol. 136, no. 2, Article ID 024706, 2012.

[4] M. J. Muñoz-Batista, M. N. Gómez-Cerezo, A. Kubacka, D. Tudela, and M. Fernández-García, "Role of interface contact in CeO_2-TiO_2 photocatalytic composite materials," *ACS Catalysis*, vol. 4, no. 1, pp. 63–72, 2014.

[5] S. Yang and L. Gao, "New method to prepare nitrogen-doped titanium dioxide and its photocatalytic activities irradiated by visible light," *Journal of the American Ceramic Society*, vol. 87, no. 9, pp. 1803–1805, 2004.

[6] X.-X. Xue, W. Ji, Z. Mao et al., "SERS study of co-doped TiO_2 nanoparticles," *Chemical Research in Chinese Universities*, vol. 29, no. 4, pp. 751–754, 2013.

[7] A. W. Tan, B. Pingguan-Murphy, R. Ahmad, and S. A. Akbar, "Advances in fabrication of TiO_2 nanofiber/nanowire arrays toward the cellular response in biomedical implantations: a review," *Journal of Materials Science*, vol. 48, no. 24, pp. 8337–8353, 2013.

[8] A. Bumajdad, M. Madkour, Y. Abdel-Moneam, and M. El-Kemary, "Nanostructured mesoporous Au/TiO_2 for photocatalytic degradation of a textile dye: the effect of size similarity of the deposited Au with that of TiO_2 pores," *Journal of Materials Science*, vol. 49, no. 4, pp. 1743–1754, 2014.

[9] S. S. Mali, C. S. Shim, H. K. Park, J. Heo, P. S. Patil, and C. K. Hong, "Ultrathin atomic layer deposited TiO_2 for surface passivation of hydrothermally grown 1D TiO_2 nanorod arrays for efficient solid-state perovskite solar cells," *Chemistry of Materials*, vol. 27, no. 5, pp. 1541–1551, 2015.

[10] D. V. Bavykin, L. Passoni, and F. C. Walsh, "Hierarchical tube-in-tube structures prepared by electrophoretic deposition of nanostructured titanates into a TiO_2 nanotube array," *Chemical Communications*, vol. 49, no. 62, pp. 7007–7009, 2013.

[11] J. Y. Kim, K. Zhu, N. R. Neale, and A. J. Frank, "Transparent TiO_2 nanotube array photoelectrodes prepared via two-step anodization," *Nano Convergence*, vol. 1, article 9, 2014.

[12] K. Lee, R. Kirchgeorg, and P. Schmuki, "Role of transparent electrodes for high efficiency TiO_2 nanotube based dye-sensitized solar cells," *The Journal of Physical Chemistry C*, vol. 118, no. 30, pp. 16562–16566, 2014.

[13] H. Cui, W. Zhao, C. Yang et al., "Black TiO_2 nanotube arrays for high-efficiency photoelectrochemical water-splitting," *Journal of Materials Chemistry A*, vol. 2, no. 23, pp. 8612–8616, 2014.

[14] T. H. T. Vu, H. T. Au, L. T. Tran et al., "Synthesis of titanium dioxide nanotubes via one-step dynamic hydrothermal process," *Journal of Materials Science*, vol. 49, no. 16, pp. 5617–5625, 2014.

[15] A. Mohammadpour and K. Shankar, "Magnetic field-assisted electroless anodization: TiO_2 nanotube growth on discontinuous, patterned Ti films," *Journal of Materials Chemistry A*, vol. 2, no. 34, pp. 13810–13816, 2014.

[16] D. A. H. Hanaor and C. C. Sorrell, "Review of the anatase to rutile phase transformation," *Journal of Materials Science*, vol. 46, no. 4, pp. 855–874, 2011.

[17] D. Tahk, T.-I. Kim, H. Yoon, M. Choi, K. Shin, and K. Y. Suh, "Fabrication of antireflection and antifogging polymer sheet by partial photopolymerization and dry etching," *Langmuir*, vol. 26, no. 4, pp. 2240–2243, 2010.